available at www.sciencedirect.com

ScienceDirect

journal homepage: www.elsevier.com/locate/chnjc

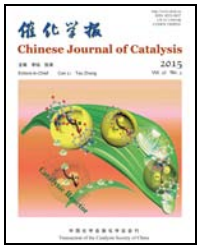

Article

In-situ synthesis of C_3N_4/CdS composites with enhanced photocatalytic properties

Yanjuan Cui *

School of Environmental and Chemical Engineering, Jiangsu University of Science and Technology, Zhenjiang 212003, Jiangsu, China

ARTICLE INFO

Article history:
Received 31 August 2014
Accepted 8 October 2014
Published 20 March 2015

Keywords:
Carbon nitride
Cadmium sulfide
Photocatalysis
Degradation of pollutants

ABSTRACT

A hybrid semiconductor composed of a carbon nitride/cadmium sulfide nanocomposite (C_3N_4/CdS) was synthesized by a template-free one-step calcination route at high temperature using ammonium thiocyanate and cadmium chloride as starting materials. The crystal structure, composition and morphology of the hybrid samples were studied by X-ray diffraction, Fourier transform infrared spectroscopy and transmission electron microscopy. The photocatalytic degradation of Rhodamine B as a model compound was carried out to evaluate the photocatalytic activity of the nanocomposites under visible light irradiation. Hexagonal CdS nanocrystals were uniformly distributed in the bulk C_3N_4. After coupling with CdS the basic C_3N_4 structure was mostly unchanged. The visible light absorption properties of the hybrid materials were enhanced. The as-prepared C_3N_4/CdS hybrid photocatalyst exhibited superior degradation performance under visible light irradiation compared with pure C_3N_4. The well-matched band energy improved the transfer efficiency of the photoinduced carriers and this was responsible for the enhanced photocatalytic activity and stability of the hybrid photocatalysts.

1. Introduction

Graphite carbon nitride (g-C_3N_4) has attracted much attention as a metal-free polymer semiconductor in the field of functional materials. In 2009, Wang et al. [1] were the first to report that C_3N_4 can be used as a photocatalyst for hydrogen evolution from water. This nonmetal semiconductor has attracted much interest. Based on its low cost, availability, simple synthesis process, suitable energy band structure, visible light response, environmentally friendly nature and the absence of secondary pollution, it has become the focus of much research in the materials and chemistry disciplines. Several studies have shown that C_3N_4 has potential application in many fields such as precursor materials for the preparation of nitrides [2], catalyst carriers [3], energy storage materials [4], sensors [5], organic catalysts [6], and photocatalysts [7–10]. As a visible light response catalyst, C_3N_4 is widely discussed in the fields of energy photocatalysis, environmental photocatalysis, selective organic optical synthesis, and the photocatalytic preparation of polymers.

However, because of the nature of the polymer material (high exciton binding energy of 1.5–2 eV), the photogenerated electron-hole pairs in C_3N_4 semiconductor separate with difficulty. The poor carrier mobility in this polymer material results in a low quantum efficiency during the photocatalytic reaction process. Additionally, the band gap of C_3N_4 is about 2.7 eV and thus it can only be excited by light with wavelengths less than 460 nm during photocatalytic applications. This does not allow

* Corresponding author. Tel/Fax: +86-511-85605157; E-mail: yjcui@just.edu.cn
This work was supported by the Natural Science Foundation of Jiangsu Province (BK20140507).
DOI: 10.1016/S1872-2067(14)60237-0 | http://www.sciencedirect.com/science/journal/18722067 | Chin. J. Catal., Vol. 36, No. 3, March 2015

for the full use of visible light. The band positions of C_3N_4 are at about −1.3 and 1.4 V (vs NHE, pH = 7) with regard to the conduction band (CB) and the valence band (VB), respectively. From the thermodynamic analysis, the oxidation capacity of C_3N_4 is limited by its high oxidation potential. Hydroxyl radicals are therefore not generated from water during photo-oxidation. This results in insufficient oxidation capacity and inefficient photocatalytic degradation of organic pollutants in wastewater. Therefore, the limited visible light absorption, the high recombination rate of photogenerated charges and the low oxidation potential are serious impediments for the application of C_3N_4 in environmental purification [11–13].

Based on this analysis of the disadvantages of C_3N_4, the design, synthesis, and modification of novel C_3N_4 based photocatalysts are inevitable for researchers. Currently, much work has been carried out on C_3N_4 modification such as precious metal deposition [14], doping with metal/nonmetal ions [15,16], and semiconductor compositions [17,18]. Coupling other semiconductors (typically TiO_2) [19] with C_3N_4 is a simple method to improve its photocatalytic performance and advantage is taken of current mature semiconductor materials. Diverse semiconductors (ultraviolet or visible light response) coupled with C_3N_4 have also been investigated. For example, a C_3N_4/ZnO heterojunction was obtained by different methods and the results showed that the photocatalytic activity and stability of this composite were higher than those of the single components [20]. Fu and co-workers [21] prepared BiOBr-g-C_3N_4 hybrid material and this composite was able to separate and transfer photogenerated charge effectively. The photocatalytic degradation efficiency of this new material toward Rhodamine B (RhB) improved 17.2-fold compared with pure C_3N_4, and after 8 cycles it retained its good stability and its activity did not decrease. Multiple composite materials based on C_3N_4 have also been reported. Ternary Ag/Ag_3PO_4/g-C_3N_4 hybrid photocatalysts were prepared and they showed enhanced photodegradation activity toward RhB in solution [22].

Cadmium sulfide (CdS) has always been considered a visible light response semiconductor material with good photocatalytic performance. However, a photocorrosion phenomenon because of serious self-oxidation by photogenerated holes greatly limits its application in the field of photocatalysis. Research interest in this material has never subsided. The synthesis of CdS nanocrystals or the construction of heterojunction structures to accelerate the migration rate of photogenerated holes has been successful in overcoming this problem [23–26]. A comparison of the band gap edges of C_3N_4 and CdS revealed that their band structures matched well and a heterojunction could be constructed between these materials to improve the separation and transfer efficiency of photoinduced carriers. The preparation of novel photocatalyst C_3N_4/CdS composite materials is promising in overcoming the disadvantages of C_3N_4 and CdS. Recently, a composite consisting of C_3N_4 and CdS coupled quantum dots was synthesized by Ge et al. [27]. Their results showed that this catalyst extended the range of visible light absorption to 550 nm and its fluorescence intensity decreased significantly compared with C_3N_4. This indicates a significant induced recombination of photogenerated electrons and holes. The catalytic efficiency of this hybrid sample was much higher than that of the single components. A C_3N_4/CdS material was also obtained by Fu et al. [28] using the deposition-precipitation method, and its activity toward the visible light photocatalytic degradation of methyl orange and 4-amino benzoic acid increased significantly. All these study results show that C_3N_4/CdS composites are efficient materials and they have research and application value in the photocatalytic degradation of environmental pollutants.

However, few reports exist in which C_3N_4 has been coupled with CdS nanocrystals in a template-free one-step route. In our previous report, ammonium thiocyanate was used to synthesize C_3N_4 but with sulfur loss during the preparation process. Herein, we describe a new preparation method for the C_3N_4/CdS hybrid material containing CdS nanocrystals. A detailed investigation into the catalytic activity was carried out with RhB as a model contaminant. We found that the C_3N_4/CdS hybrid system exhibited superior photocatalytic performance toward RhB degradation with good stability under visible light irradiation compared with individual C_3N_4 components. Its enhanced photoactivity can be attributed to improved visible light absorption and rapid electron-hole pair separation. This work is a continuation of our commitment to the development of C_3N_4 based composite semiconductors with high efficiency and stability for use in environmental purification by photocatalytic techniques.

2. Experimental

2.1. Catalyst preparation

All the materials were purchased from Sinopharm Chemical Reagent Co., Ltd. (Shanghai, China) and used as received without further purification.

C_3N_4/CdS samples were synthesized by mixing NH_4SCN (15 g) with different amounts of $CdCl_2{\cdot}2.5H_2O$ in 15 mL water with stirring at 80 °C to remove water. After thorough drying in an oven at 60 °C, the resultant solids were calcined at 550 °C for 2 h at a ramp rate of 8 °C/min in N_2 atmosphere to yield yellow samples [29]. The obtained samples were denoted $C_3N_4/CdS_{x\text{-}T}$, where x (x = 0, 0.1%, 0.3%, 0.5%, 1%, 2%) refers to the initial mass ratio of $NH_4SCN/CdCl_2{\cdot}2.5H_2O$ and T refers to the calcination temperature. The yield of C_3N_4 obtained using NH_4SCN as a precursor was about 12% and according to the elemental analysis results, the real mass ratio of CdS to C_3N_4 in the composites was about 2% for $C_3N_4/CdS_{1\%\text{-}550}$, for example. Catalysts were prepared at 550 °C unless otherwise noted.

2.2. Catalyst characterization

X-ray diffraction (XRD) measurements were obtained on a Bruker D8 Advance diffractometer with Cu K_α radiation (λ = 0.15406 nm). Fourier transform infrared (FTIR) spectra were recorded using a Nicolet Magna 670 FTIR spectrometer in KBr at a concentration of ca. 1 wt%. UV-Vis diffuse reflectance spectra (DRS) were obtained on a Varian Cary 500 Scan UV-visible system. The chemical compositions of the prepared

samples were measured by elemental analysis (Vario MICRO) and ICP (Ultima2). X-ray photoelectron spectroscopy (XPS) data were obtained on a Thermo ESCALAB250 instrument with a monochromatized Al K_α line source (200 W). Transmission electron microscopy (TEM) was carried out using a JEOL model JEM 2010 EX instrument. The photoluminescence (PL) emission spectra were obtained on a FS/FL920 time-resolved fluorescence spectrometer.

2.3. Photocatalytic tests

The degradation of RhB solution (10^{-5} mol/L) was used as a model reaction to evaluate the photodegradation behavior of the C_3N_4/CdS hybrid photocatalyst. The light source for the photocatalytic reaction was a 500-W halogen lamp. Combined cutoff filters were used to remove wavelengths below 420 nm and above 800 nm. In each experiment, 40 mg photocatalyst was added into 80 mL model pollutant solution. After reaching the adsorption-desorption equilibrium within 0.5 h, 3 mL of the suspensions were collected at different irradiation time intervals and then centrifuged to remove the photocatalyst particles. The change in RhB concentration was determined by UV-Vis spectroscopy using a Cary 50 UV-Vis spectrophotometer.

3. Results and discussion

3.1. Structural characterization

Fig. 1 shows XRD patterns of the CdS/C_3N_4 hybrid photocatalysts that were prepared at 550 °C with different CdS contents. For all the samples, the distinctive diffraction peaks of C_3N_4 were present at 13.0° (d = 0.618 nm) and 27.4° (d = 0.326 nm). These correspond to (001) in-planar repeat tri-s-triazine units and the (002) interlayer reflection of C_3N_4 [30]. With an increase in the proportion of CdS in the composite material, the CdS diffraction peaks became stronger and that of C_3N_4 became broader and weaker. This indicates that the degree of C_3N_4 polymerization was hindered to some extent because of the participation of CdS crystals, however, its main structure remained unchanged.

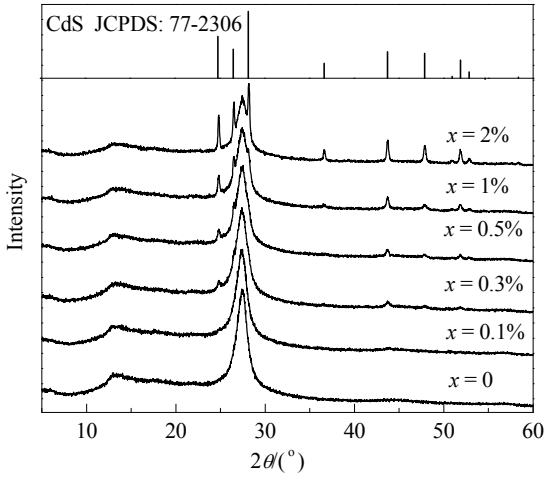

Fig. 1. XRD patterns of different C_3N_4/CdS_x samples.

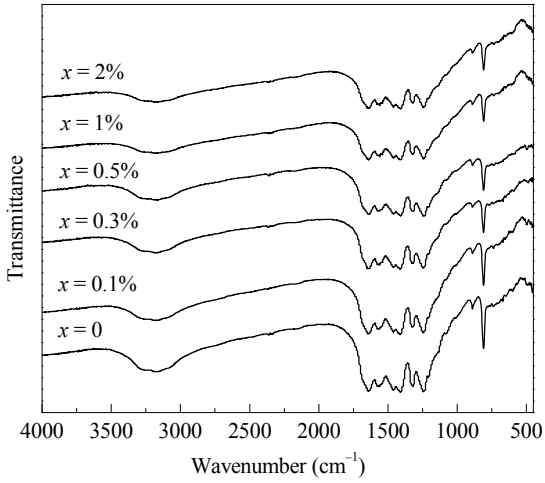

Fig. 2. FTIR spectra of different C_3N_4/CdS_x samples.

The diffraction peaks of CdS were not clear in C_3N_4/$CdS_{0.1\%}$. This may be due to the low amount and highly dispersed CdS of small particle size. With an increase in the content of CdS in the composite samples, new CdS diffraction peaks appeared. For C_3N_4/$CdS_{1\%}$, strong peaks that correspond to the (002), (110), and (112) planes of the hexagonal phase CdS (JCPDS 77-2306) were present. The weak peak intensity and the wide half peak width imply small CdS nanoparticles. These results indicate that hexagonal phase CdS nanocrystals were well mixed with the bulk C_3N_4 from this one-step synthesis route.

FTIR spectra of the as-synthesized C_3N_4/CdS hybrid photocatalysts are shown in Fig. 2. The broad absorption band at 3100–3300 cm^{-1} can be assigned to the stretching modes of secondary and primary amines and their intermolecular hydrogen-bonding interactions. The band at 810 cm^{-1} belongs to s-triazine ring modes and the bands at 1200–1600 cm^{-1} are characteristic of aromatic carbon nitride heterocycles. All the products synthesized in solution at different temperatures are characterized by a series of bands in the 1200–1700 cm^{-1} region and a strong peak at approximately 800 cm^{-1} [31]. These IR bands are typical molecular vibration modes of triazine rings. Symmetric and antisymmetric $-NH_2$ stretching modes were found in the high-frequency region at approximately 3300 cm^{-1}. These results indicate that the structure of C_3N_4 was not changed upon the inclusion of CdS nanocrystals.

TEM was used for a comprehensive analysis of the texture and crystal structure of the hybrid samples. From Fig. 3, the presence of CdS crystal particles with clear lattice fringes was

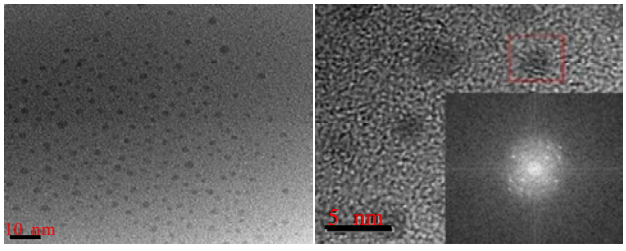

Fig. 3. Typical HRTEM images of C_3N_4/$CdS_{1\%}$. Inset shows corresponding fast Fourier transforms of the patterns.

evident and they were well dispersed in the hybrid sample. The particle size was uniform at about 3–8 nm.

For the crystal particles, notable diffraction spots with a cmm symmetry distribution were found using a high-resolution Fourier transform. A further analysis of these diffraction spots indicated that they belonged to the (101), (110) and (103) planes of CdS. The crystal plane spacings were 0.32, 0.21, and 0.16 nm, respectively. This is typical of hexagonal CdS crystals and confirms the presence of CdS nanocrystals in the hybrid catalysts, which is consistent with the XRD patterns.

XPS studies were carried out to investigate the structural environments of the constituent elements in the C_3N_4/CdS samples. Fig. 4 shows XPS spectra of C_3N_4/$CdS_{1\%}$. Signals from C, N, O that belong to C_3N_4 are present in the spectrum (Fig. 5(a)) but signals for CdS are not present. This indicates that the CdS nanocrystals were well dispersed in the C_3N_4 bulk and that not much coupling occurred on the surface of C_3N_4. Higher resolution spectra were obtained for the C1*s*, N1*s* and Cd 2*p* regions. The C1*s* spectrum contains two peaks centered at 288.0 and 284.6 eV. The main contributing peak at 288.0 eV originates from sp^2 hybridized carbon in the aromatic ring. The C1*s* peak at 284.6 eV is typically assigned to graphitic carbon or sp^2 C–N [32]. The N1*s* spectra can be deconvoluted into three peaks. The main component centered at 398.2 eV is attributed to sp^2 N from the triazine rings whereas the contribution at 400.1 eV corresponds to the bridging N atoms N–(C)3 [33]. The peak at 404.1 eV comes from charging effects or positive charge localization in the heterocycles [34]. The high-resolution fitting peaks for C and N are consistent with our previous work. They indicate that the presence of CdS particles did not change the composition or the basic chemical structure of C_3N_4. Additionally, the characteristic Cd 3*d* peak was present at 405.7 eV. This peak was lower than the standard XPS binding energy (408.0 eV) for Cd^{2+} 3*d*, which indicates an increase in the electron density of CdS [35]. This may be caused by electron transfer from C_3N_4 to CdS because of the energy difference between them.

The optical features of the as-prepared hybrid C_3N_4/CdS materials were examined by UV-Vis DRS, as shown in Fig. 5. It is obvious that all the curves had a steep absorption edge at about 465 nm, which means that all the samples undergo semiconductor absorption in the visible light region. In contrast to the spectrum of pure C_3N_4, the absorption band edge red-shifted slightly and the absorption of visible light improved for the C_3N_4/CdS samples, especially from 460 to 520 nm. Although not very significant, the improvement in light absorption may improve the efficiency of visible light utilization. This is attributed to the narrow band gap of CdS and the strong heterogeneous interaction between C_3N_4 and CdS. The band gap of C_3N_4 is about 2.7 eV, which corresponds to an absorption band edge around 465 nm. The band gap of CdS is about 2.4 eV, which corresponds to a wavelength of about 520 nm [36,37].

Room temperature PL spectra were obtained using excitation light of 365 nm to investigate the efficiency of charge- carrier separation/recombination in the hybrid materials. As

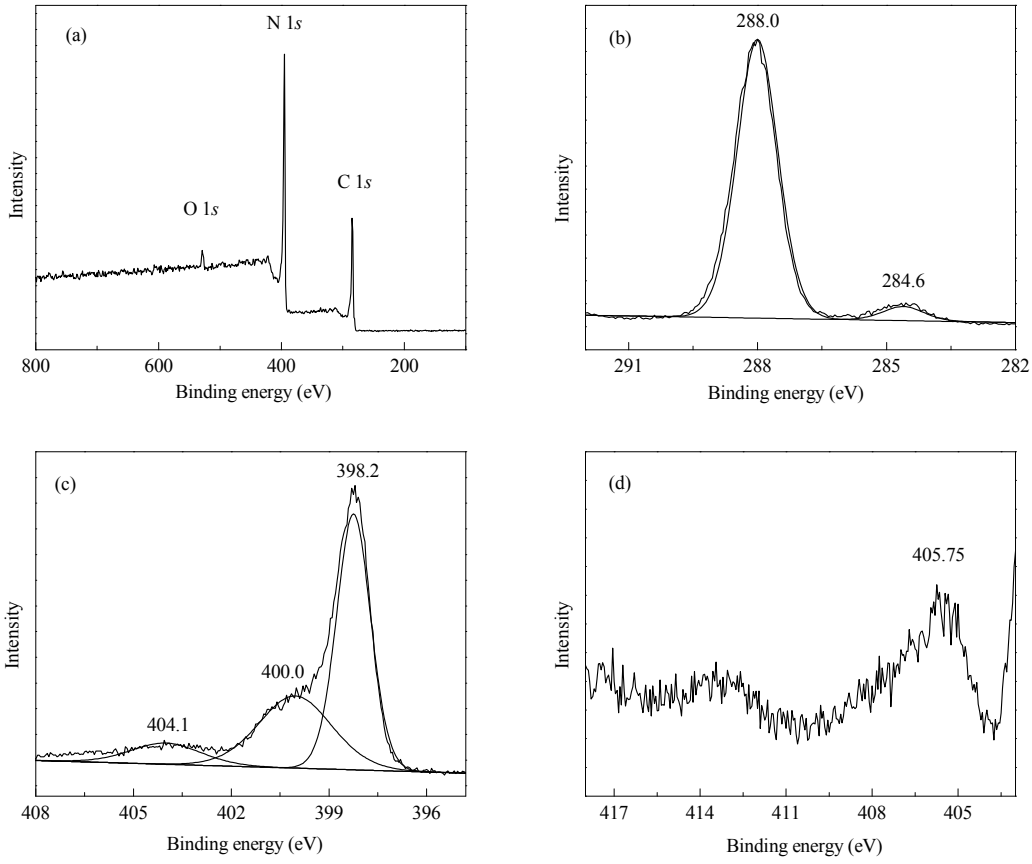

Fig. 4. XPS survey spectrum of C_3N_4/$CdS_{1\%}$ (a) and corresponding high-resolution XPS spectra of C 1*s* (b), N 1*s* (c) and Cd 2*p* (d).

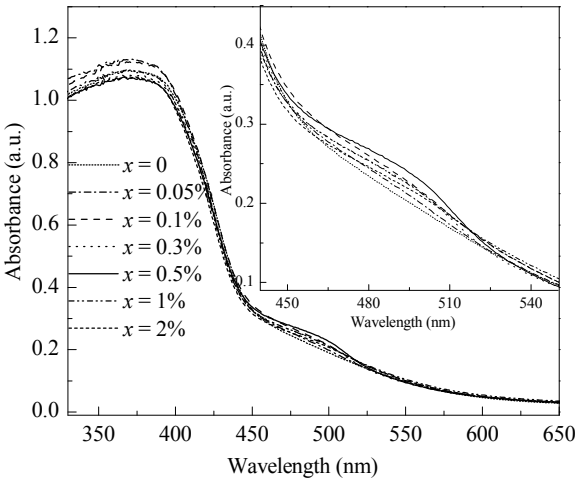

Fig. 5. UV-Vis absorption spectra of the C_3N_4 and different C_3N_4/CdS_x samples.

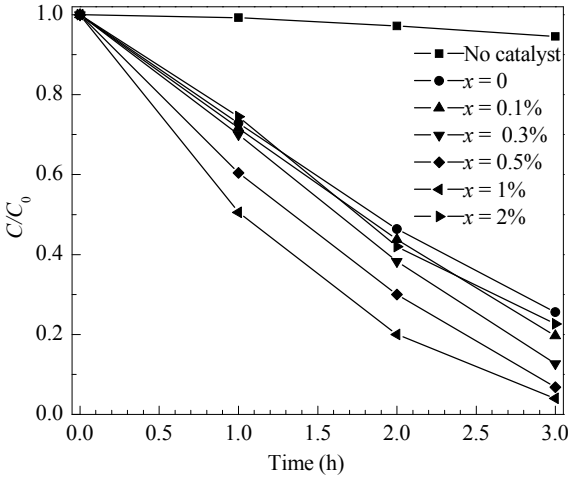

Fig. 7. Photocatalytic degradation of RhB over different C_3N_4/CdS_x samples obtained at 550 °C under visible light irradiation.

shown in Fig. 6, all the samples exhibited a broad emission peak centered around 460 nm and this can be attributed to the band-band PL phenomenon with the light energy approximately equal to the band gap energy (2.7 eV) of C_3N_4 [38]. The PL intensity of C_3N_4 decreased after coupling with CdS nanocrystals, and it continuously decreased as the CdS content increased. In principle, PL quenching indicates a suppressed recombination rate of photoinduced charge carriers. The main benefit comes from the construction of the heterojunction structure, which hastens the mobility of the free charge carriers [39–41]. The lower recombination rate of the charge carriers facilitates heterogeneous photocatalysis.

3.2. Photocatalytic performance

The photocatalytic activity of the hybrid C_3N_4/CdS catalysts with different CdS contents was determined by an analysis of the degradation of the organic dye RhB under visible light irradiation. The results are shown in Fig. 7. In contrast to pure C_3N_4, the photocatalytic degradation activity of C_3N_4/CdS improved with an increase in CdS composite content. However, the catalysts with higher CdS content did not possess higher activity. In this work, the CdS nanocrystals hybridized uniformly in the C_3N_4 bulk instead of coupling to the surface of C_3N_4 as reported before. Therefore, heterojunction structures were present throughout the material, not just on the surface of the catalysts. Therefore, a small amount of CdS improved the photocatalytic activity obviously. The $C_3N_4/CdS_{1\%}$ catalyst gave the best degradation activity. With an increase in CdS content the photocatalytic activity of $C_3N_4/CdS_{2\%}$ decreased. This may be due to the formation of recombination centers of photoinduced carriers in the bulk of the catalyst.

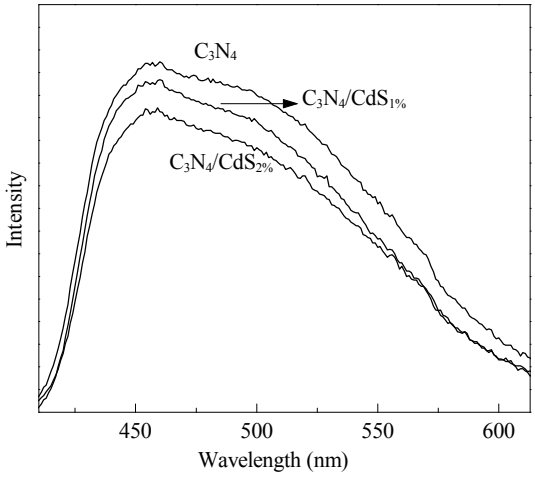

Fig. 6. PL spectra of the C_3N_4 and C_3N_4/CdS samples.

In this work, controlled experiments were also carried out to demonstrate the heterojunction effect in the hybrid catalyst. 1 mg CdS and a mechanically mixed composite of 39 mg C_3N_4 and 1 mg CdS were used as photocatalysts for the RhB degradation tests. Only ~10% of the RhB was removed by CdS over the same irradiation time. The degradation rate of the mixed catalysts was almost the same as that of pure C_3N_4. Although pure CdS had good photocatalytic activity toward the photocatalytic degradation of pollutants, its own catalytic action was almost negligible because only trace amounts of CdS were present in this hybrid catalyst.

To determine the influence of preparation conditions on the photocatalytic activity of C_3N_4/CdS, the $C_3N_4/CdS_{1\%}$ samples were synthesized at different temperatures. Their corresponding photocatalytic activity was determined and the results are shown in Fig. 8(a) and 8(b). The results show that the photocatalytic activity of the two samples synthesized at 500 °C below was low with little difference. However, when the calcination temperature was increased (> 550 °C), the activity of these two types of catalysts improved. In particular, the catalytic activity of C_3N_4/CdS was much higher than that of pure C_3N_4 that was prepared at the same temperature.

The RhB degradation process was fit using quasi first-order kinetics, and the rate constants are listed in Fig. 8(c). For pure C_3N_4, the catalytic activity increased for the higher calcination temperature samples but the effect was limited. For the C_3N_4/CdS materials, the improvement in photocatalytic activity

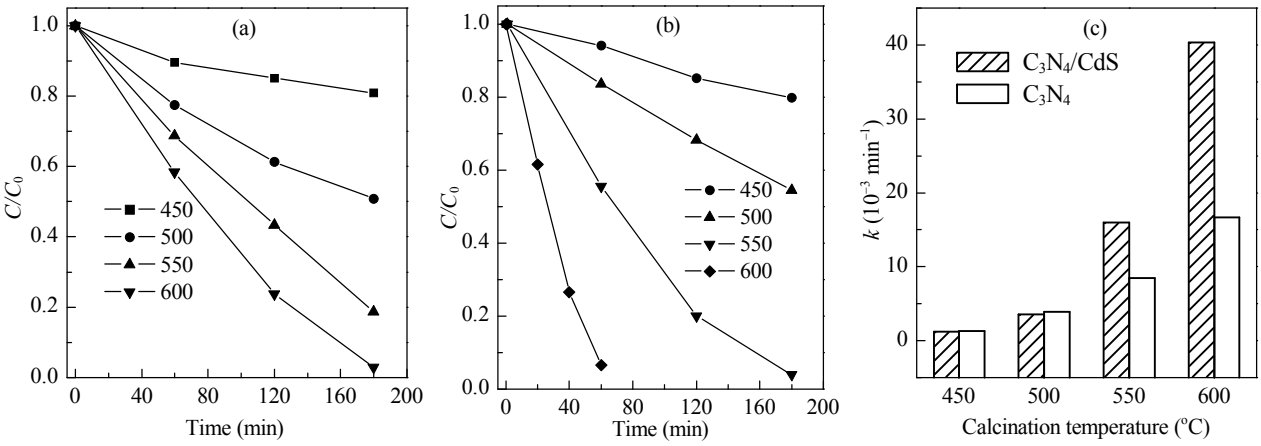

Fig. 8. Photocatalytic activity of C_3N_4 (a) and $C_3N_4/CdS_{1\%}$ (b) prepared at different temperatures and the photocatalytic degradation rate constant of RhB after irradiation for 3 h over the prepared catalysts (c).

was more significant. For the samples synthesized at 600 °C below, the rate constant for RhB degradation over C_3N_4/CdS was about 1.5 times that of pure C_3N_4. Based on our previous studies, the defects that promote electron localization can increase in bulk C_3N_4 prepared at higher temperature [42].

To determine the photostability of the hybrid catalysts, the photocatalytic degradation of RhB over $C_3N_4/CdS_{1\%\text{-}600}$ was repeated for up to five cycles under the same conditions. After five successive operations, the catalyst retained its high photocatalytic RhB degradation activity and no apparent decrease in photocatalytic activity (Fig. 9) was evident. A composition analysis of the used catalyst also showed that the CdS content was mostly unchanged (Table 1). These results indicate that the hybrid photocatalyst was stable under the experimental reaction conditions.

A proposed mechanism for the separation and transport of the photogenerated charges at the interface of C_3N_4/CdS during the photocatalytic process is shown in Fig. 10. From literature, the CB and VB potentials of CdS are estimated to be −0.4 and 1.8 eV while the CB and VB potentials of C_3N_4 are −1.3 and 1.4 eV [14]. The band positons of C_3N_4 and CdS meet the requirements of well-matched heterostructures. Under visible light irradiation (λ > 420 nm), both C_3N_4 and CdS can be excited to produce photogenerated electrons (e^-) and holes (h^+). With the closely connected interfaces and the well-matched overlapping band structure, the electrons in the CB of C_3N_4 can transfer to the CB of CdS directly, and the holes in the VB of CdS can move to the VB of C_3N_4 spontaneously. The active oxygen species $\bullet O_2^-$ (generated from O_2 and e^-) and the holes can then oxidize the organic substrates resulting in decomposition products. In this process, an improved charge separation efficiency reduces the probability of charge recombination. The self-oxidation of CdS by holes is thus mostly prevented. As a result, the photocatalytic activity and stability of this composite material increases.

Table 1
Composition ratio of the elements in the as-prepared samples.

Sample	*w*(C)%	*w*(N)%	*w*(H)%	*w*(Cd)%	*w*(S)%
C_3N_4	35.6	55.4	2.5	—	0.09
$C_3N_4/CdS_{0.5\%\text{-}550}$	34.8	54.7	2.4	1.6	0.4
$C_3N_4/CdS_{1\%\text{-}550}$	34.5	54.1	2.4	2.5	0.7
$C_3N_4/CdS_{2\%\text{-}550}$	34.6	53.6	2.5	4.7	1.2
$C_3N_4/CdS_{1\%\text{-}600}$	33.4	51.8	2.4	2.6	0.7
$C_3N_4/CdS_{1\%\text{-}600}$ used	33.2	51.6	2.5	2.5	0.7

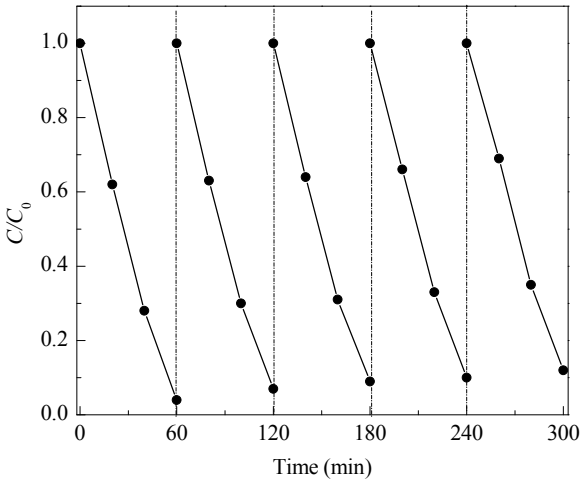

Fig. 9. Stability of $C_3N_4/CdS_{1\%\text{-}600}$ during RhB degradation under visible light irradiation.

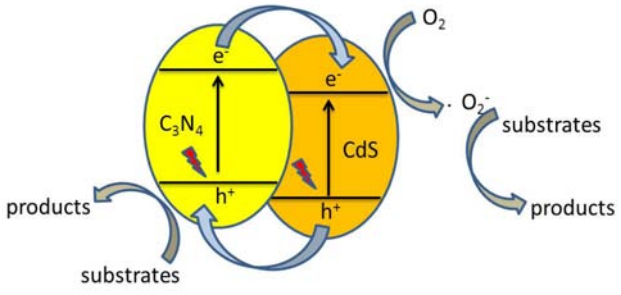

Fig. 10. Schematic of photogenerated charge transfer in the C_3N_4/CdS system under visible light irradiation.

Graphical Abstract

Chin. J. Catal., 2015, 36: 372–379 doi: 10.1016/S1872-2067(14)60237-0

In-situ synthesis of C_3N_4/CdS composites with enhanced photocatalytic properties

Yanjuan Cui*
Jiangsu University of Science and Technology

C_3N_4/CdS nanocomposites with CdS nanocrystals uniformly dispersed in the bulk of C_3N_4 were synthesized using a one-step calcination method. They were shown to be stable hybrid photocatalysts for the degradation of organic pollutants under visible light irradiation.

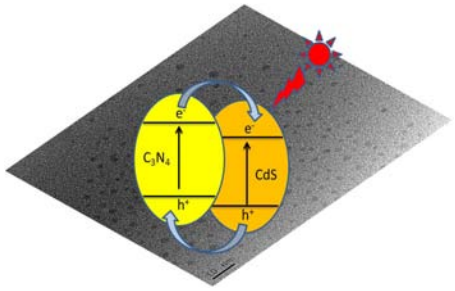

4. Conclusions

A hybrid catalyst C_3N_4/CdS with low CdS content was successfully synthesized by a template-free one-step method using NH_4SCN and $CdCl_2$ as precursors. In this composite material, hexagonal CdS nanocrystals with a particle size of about 5 nm were uniformly distributed in the bulk of C_3N_4. A well-constructed heterojunction between C_3N_4 and CdS resulted in the visible light absorption intensity of the hybrid materials improving and the separation rates of the photo-excited carriers accelerating because a good match was obtained for the energy band structure between them. Under visible light irradiation, the photocatalytic degradation of RhB on the hybrid samples improved compared with the pure C_3N_4 catalyst. The composite content of CdS and the preparation temperature greatly influenced the photocatalytic activity of the C_3N_4/CdS samples. $C_3N_4/CdS_{1\%\text{-}600}$ gave the best photocatalytic activity under the experimental conditions and good stability was maintained during repeated use. This work demonstrates that a one-step synthesis of carbon nitride based composite semiconductors modified with small amounts of metal sulfides giving high photocatalytic efficiency and good stability is possible. In this work, the improvement in photocatalytic degradation activity was not particularly significant, and further work is required to optimize the composite structure of the catalyst.

References

[1] Wang X C, Maeda K, Chen X F, TakaNabe K, Domen K, Hou Y D, Fu X Z, Antonietti M. *J Am Chem Soc*, 2009, 131: 1680
[2] Fischer A, Antonietti M, Thomas A. *Adv Mater*, 2007, 19: 264
[3] Kim M, Hwang S, Yu J S. *J Mater Chem*, 2007, 17: 1656
[4] Park S S, Chu S W, Xue C F, Zhao D Y, Ha C S. *J Mater Chem*, 2011, 21: 10801
[5] Lee E Z, Jun Y S, Hong W H, Thomas A, Jin M M. *Angew Chem Int Ed*, 2010, 49: 9706
[6] Goettmann F, Fischer A, Antonietti M, Thomas A. *Angew Chem Int Ed*, 2006, 45: 4467
[7] Wang Y, Wang X C, Antonietti M. *Angew Chem Int Ed,* 2012, 51: 68
[8] Zheng Y, Liu J, Liang J, Jaroniec M, Qiao S Z. *Energy Environ Sci*, 2012, 5: 6717
[9] Zhang J S, Grzelczak M, Hou Y D, Maeda K, Domen K, Fu X Z, Antonietti M, Wang X C. *Chem Sci*, 2012, 3: 443
[10] Cao S W, Yu J G. *J Phys Chem Lett*, 2014, 5: 2101
[11] Yan S C, Li Z S, Zou Z G. *Langmuir*, 2010, 26: 3894
[12] Lee S C, Lintang H O, Yuliati L. *Chem Asian J*, 2012, 7: 2139
[13] Shalom M, Inal S, Fettkenhauer C, Neher D, Antonietti M. *J Am Chem Soc*, 2013, 135: 7118
[14] Li X H, Antonietti M. *Chem Soc Rev*, 2013, 42: 6593
[15] Ye X J, Cui Y J, Wang X C. *ChemSusChem*, 2014, 7: 738
[16] Zhang Y J, Mori T, Ye J H, Antoniett M. *J Am Chem Soc*, 2010, 132: 6294
[17] Wang W J, Yu J C, Xia D H, Wong P K, Li Y C. *Environ Sci Technol*, 2013, 47: 8724
[18] Pan C S, Xu J, Wang Y J, Li D, Zhu Y F. *Adv Funct Mater*, 2012, 22: 1518
[19] Yu J G, Wang S H, Low J X, Xiao W. *Phys Chem Chem Phys*, 2013, 15: 16883
[20] Sun J X, Yuan Y P, Qiu L G, Jiang X, Xie A J, Shen Y H, Zhu J F. *Dalton Trans*, 2012, 41: 6756
[21] Fu J, Tian Y L, Chang B B, Xi F N, Dong X P. *J Mater Chem*, 2012, 22: 21159
[22] Shen K, Gondal M A, Siddique R G, Shi S, Wang S Q, Sun J B, Xu Q Y. *Chin J Catal* (沈凯, Gondal M A, Siddique R G, 施珊, 王斯琦, 孙江波, 徐庆宇. 催化学报), 2014, 35: 78
[23] Hu Y, Gao X H, Yu L, Wang Y R, Ning J Q, Xu S J, Lou X W. *Angew Chem Int Ed*, 2013, 52: 5636
[24] Hirai T, Bando Y, Komasawa I. *J Phys Chem B*, 2002, 106: 8967
[25] Tang Z R, Yin X, Zhang Y H, Xu Y J. *Inorg Chem*, 2013, 52: 11758
[26] Zong X, Wu G P, Yan H J, Ma G J, Shi J Y, Wen F Y, Wang L, Li C. *J Phys Chem C*, 2010, 114: 1963
[27] Ge L, Zuo F, Liu J K, Ma Q, Wang C, Sun D Z, Bartels L, Feng P Y. *J Phys Chem C*, 2012, 116: 13708
[28] Fu J, Chang B B, Tian Y L, Xi F N, Dong X P. *J Mater Chem A*, 2013, 1: 3083
[29] Cui Y J, Zhang J S, Zhang G G, Huang J H, Liu P, Antonietti M, Wang X C. *J Mater Chem*, 2011, 21: 13032
[30] Cui Y J, Huang J H, Fu X Z, Wang X C. *Catal Sci Technol*, 2012, 2: 1396
[31] Lotsch B V, Schnick W. *Chem Mater*, 2006, 18: 1891
[32] Lyth S M, Nabae Y, Moriya S, Kuroki S, Kakimoto M, Ozaki J, Miyata S. *J Phys Chem C*, 2009, 113: 20148
[33] Liu J, Zhang T, Wang Z, Dawson G, Chen W. *J Mater Chem*, 2011, 21: 14398
[34] Foy D, Demazeau G, Florian P, Massiot D, Labrugere C, Goglio G. *J Solid State Chem*, 2009, 182: 165
[35] Cao S W, Yuan Y P, Fang J, Shahjamali M M, Boey F Y C, Barber J, Loo S C J, Xun C. *Int J Hydrogen Energy*, 2013, 38, 1258
[36] Bao N Z, Shen L M, Takata T, Domen K. *Chem Mater*, 2008, 20: 110
[37] Jiang D W, Zhou T S, Sun Q, Yu Y Y, Shi G Y, Jin L T. *Chin J Chem*, 2011, 29: 2505

[38] Chen X F, Jun Y S, Takanabe K, Maeda K, Domen K, Fu X Z, Antonietti M, Wang X C. *Chem Mater*, 2009, 21, 4093
[39] Zhang J S, Chen X F, Takanabe K, Maeda K, Domen K, Epping J D, Fu X Z, Antonietti M, Wang X C. *Angew Chem Int Ed*, 2010, 49: 441
[40] Zhang J S, Zhang M W, Sun R Q, Wang X C. *Angew Chem Int Ed*, 2012, 51: 10145
[41] Zhang G G, Zhang M W, Ye X X, Qiu X Q, Lin S, Wang X C. *Adv Mater*, 2014, 26: 805
[42] Cui Y J, Ding Z X, Liu P, Antonietti M, Fu X Z, Wang X C. *Phys Chem Chem Phys*, 2012, 14: 1455

原位合成具有高可见光催化活性的C_3N_4/CdS纳米复合材料

崔言娟*

江苏科技大学环境与化学工程学院, 江苏镇江212003

摘要: 以硫氰酸铵和氯化镉为原料, 采用无模板混合高温煅烧法一步合成氮化碳/硫化镉纳米晶(C_3N_4/CdS)的复合半导体材料. 采用X射线衍射、傅立叶变换红外光谱和透射电镜等技术对其结构和形貌进行了表征. 以有机污染物罗丹明B (RhB)为模拟污染物对复合催化剂的可见光催化活性进行测试. 结果表明, C_3N_4/CdS复合材料中CdS以六方相纳米晶的形式均匀分散; CdS的复合基本不改变C_3N_4主体结构及聚合度; 与纯C_3N_4相比, 复合材料在可见区的光吸收能力有所增强. 合适的能带匹配有利于光生载流子的迁移, 抑制了其复合速率. 在可见光照射下, 复合半导体能够更加快速的降解有机污染物, 且保持很好的稳定性.

关键词: 氮化碳; 硫化镉; 光催化; 污染物降解

收稿日期: 2014-08-31. 接受日期: 2014-10-08. 出版日期: 2015-03-20.

*通讯联系人. 电话/传真: (0511)85605157; 电子信箱: yjcui@just.edu.cn

基金来源: 江苏省自然科学基金(BK20140507).

本文的英文电子版由Elsevier出版社在ScienceDirect上出版(http://www.sciencedirect.com/science/journal/18722067).